JOURNAL OF MATERIALS SCIENCE 29 (1994) 2321–2327

Fracture characteristics of a particulate-reinforced metal matrix composite

M. J. HADIANFARD, J. HEALY, Y.-W. MAI
Centre for Advanced Materials Technology, Department of Mechanical Engineering, University of Sydney, New South Wales 2006, Australia

The effect of particulates on the failure mechanism of an Al–Mg–Si alloy 6061 with 20% angular alumina particles was studied. Fracture toughness tests were conducted on compact tension peak-aged specimens. The interaction of the reinforcement phase with the crack was investigated by optical microscopy and scanning electron microscopy, both on the surface and in the mid-thickness of the fractured specimen. It is shown that the fractured particles ahead of the crack tip, in particular the larger particles, play an important role in the void-initiation phase of the fracture process. Particle size and aspect ratio determine the likelihood of fracture. Some differences in the failure mechanisms have been observed between the mid-thickness and the surface of the specimen because of the difference between plane strain and plane stress fractures.

1. Introduction

Discontinuous reinforced metal matrix composites (MMCs) offer essentially isotropic properties with substantially improved strength and stiffness compared to the unreinforced alloys [1, 2]. However, some disadvantages such as poor tensile ductility and low fracture toughness have been reported [2, 3]. One of the major areas of research in MMCs is to study how the reinforcement phase affects the failure mechanisms and hence controls the fracture toughness of these materials.

Davidson [4] showed that the main reason for the lower fracture toughness in mechanically alloyed aluminium reinforced with silicon carbide particulates compared to the unreinforced alloy, was caused by the lower strain level achieved at the crack tip in the composite at incipient fracture. He also observed that voids were nucleated from subgrain boundaries rather than from the matrix/particle interface. Flom and Arsenault [5] found that the particle size and spacing between large particles could be the critical microstructural parameters controlling the fracture toughness.

The precise fracture mechanisms of MMC materials are still unclear. Some investigators suggest that interface debonding is unlikely to be the dominant fracture mechanism in Al/SiC particulate composite [6] while others observed that decohesion at the matrix/particle interface is the main mechanism [7]. Lucas *et al.* [8] have observed that in a discontinuous reinforced MMC, fracture occurs by a ductile failure process characterized by void growth and coalescence in the matrix material. In an *in situ* SEM deformation study on an aluminium MMC, Manoharan and Lewandowski [9] have shown that the main failure mechanism is by microcracking at and near the crack tip.

The present work attempted to identify the role of the reinforcing particulates on the fracture mechanisms of an alumina particulate-reinforced 6061 aluminium alloy.

2. Experimental procedure

2.1. Material and heat treatment

The material used was Duralcan-20%, a 6061 aluminium alloy matrix reinforced with 20% angular alumina particulates. It was produced by liquid metallurgy and extruded to rectangular plates, 25.5 mm thick and 75 mm wide. The microstructure of Duralcan-20% is shown in Fig. 1. The reinforcement phase consisted of alumina particles with lengths ranging from 1–45 μm, and an average length, $\bar{L}$, of 18.7 μm and an average aspect ratio (length/width $= \bar{A}$) of 1.8. Figs 2 and 3 show the size and aspect ratio distribution of particles on the polished surface

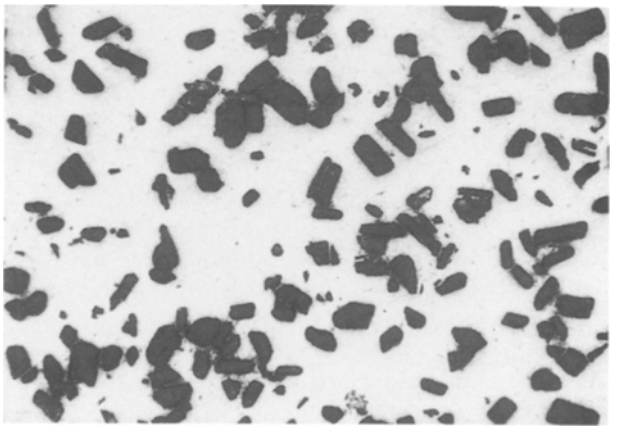

Figure 1 The microstructure of Duralcan-20%, × 350.

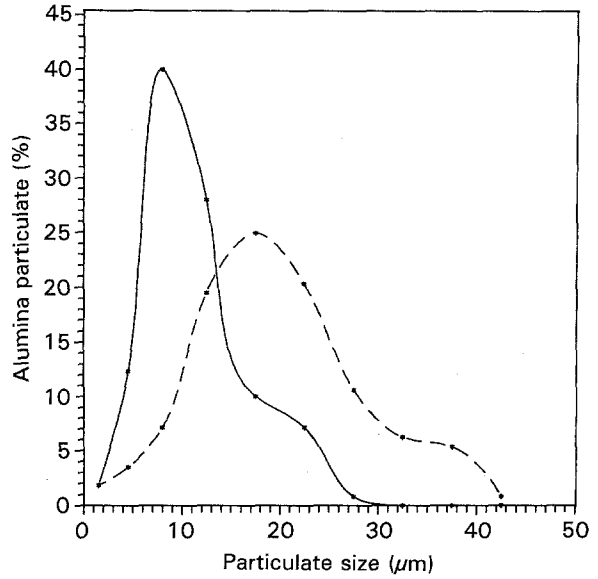

Figure 2 Distribution of particulate size on the polished surface of the as-received material: (——), width, (– – –) length.

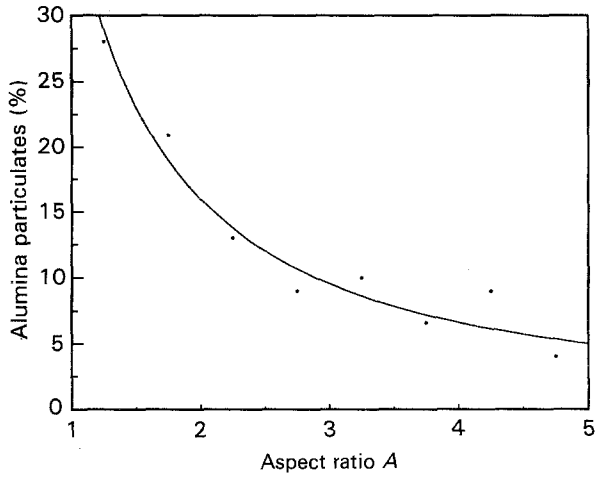

Figure 3 Distribution of particulate aspect ratio on the polished surface of the as-received material.

of the as-received MMC material. The results of an image analysis conducted on this surface indicated that 2.5% of the particles were already cracked in the as-received condition.

Specimens were cut from the plates in L – T orientation and subjected to the following heat treatments, to obtain the peak hardness condition (T6).

(a) Solution heat treated at 530 °C for 1.5 h.
(b) Cold-water quenched.
(c) Natural ageing for 24 h.
(d) Age hardening at 175 °C for 8 h.

2.2. Tensile and fracture toughness tests

Tensile testing was performed using an 1195 Instron machine. A crosshead speed of 1 mm min^{-1} was used and the load – elongation curve recorded on an $X-Y$ recorder. The elastic modulus, E, 0.2% offset yield, elongation to failure, ε_f and ultimate tensile strength (UTS) were obtained in the T6 condition.

The fracture toughness tests were carried out on compact tension (CT) specimens with a width, W, of 50 mm in accordance with E399 ASTM Standard. Three repeat tests were conducted. Precracking was performed using a 1603 Instron electromagnetic resonator.

2.3. Interrupted fracture test

A CT specimen was used to study the crack path and interaction of the crack tip with reinforcement particles. The fracture toughness test was interrupted before complete fracture could occur and two sections were machined through the mid-thickness of the specimen as illustrated in Fig. 4. These sections were polished and the crack path, in addition to the area ahead of the crack tip, on the surface and at the mid-thickness were examined by laser confocal microscopy, light microscopy and scanning electron microscopy. Optical and scanning electron micrographs were studied by means of a computer-controlled image analysis system to obtain the shape and the size of broken particles. The average length and average aspect ratio, of both fractured and unfractured particles were calculated.

2.4. Fractography and image analysis

The fracture surfaces of the CT specimens were examined using a 505 Philips scanning electron microscope and high-resolution SEM (JSM Jeol), with energy dispersive spectroscopy (EDS) capability. The micrographs obtained were subjected to detailed image analysis in order to quantify the surface features and identify the fracture mechanisms.

3. Results

3.1. Mechanical properties

The room-temperature mechanical properties for the peak-aged condition, as well as the fracture toughness, K_{Ic}, of Duralcan-20% are presented in Table I, and compared to those for the unreinforced 6061 alloy. The composite material has significantly higher strength and stiffness, and much lower ductility.

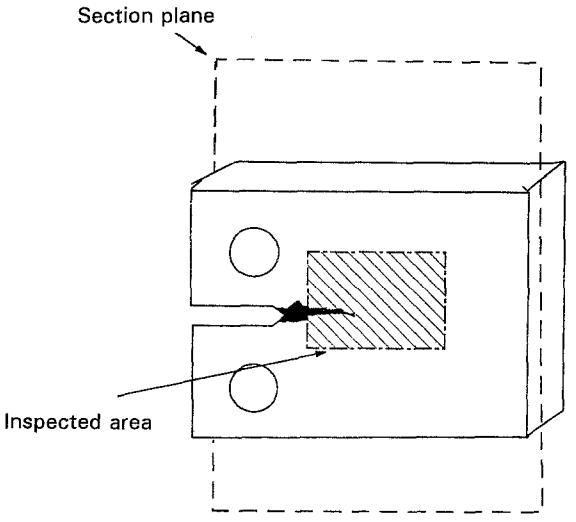

Figure 4 Schematic diagram showing the sectioning technique used to examine the surface and mid-thickness areas around and ahead of the crack tip.

TABLE I Room-temperature mechanical properties

Material	Yield stress (MPa)	UTS (MPa)	E (GPa)	ε_f (%)	K_{Ic} (MPa $m^{1/2}$)
6061 Al [19]	310	276	68.2	17	–
Duralcan 20%	335	354	97	3.2	22.8

3.2. Image analysis

Examination of the specimen surface at the tip of precrack showed that there were a large number of microcracks and fractured particles in the shear bands (Fig. 5). Although some debonded particles were also observed, most of the particles were fractured. Near the crack tip, many microcracks were found and some of these microcracks cut through the alumina particles (Fig. 6). In addition, an area with a high density of fractured particles was observed at a short distance ahead of the main crack tip (Fig. 7a and b). Statistical analysis of the geometric characteristics of these fractured particles was performed. The distribution of size and average length of fractured particles as a function of distance from crack tip are presented in Figs 8 and 9, respectively. In addition, the total average length and aspect ratio, L_t and A_t, of the fractured particles regardless of their distance from the crack tip crack are listed in Table II. A comparison of these results with those obtained from the polished surface in the as-received condition for all particles ($\bar{L} = 18.7$ μm and $\bar{A} = 1.8$) indicates that the large particles and those with a higher aspect ratio (more elongated shape) are more prone to failure than the small particles. Furthermore the average size of broken particles increases with increasing distance from the crack tip. Fig. 8 shows that while the most popular size of broken particles is between 15 and 20 μm around the crack tip, it increases to between 30 and 35 μm at a distance of 1250 μm ahead of crack tip.

In the mid-thickness of the CT specimen, the fracture path also passed through fractured particles. However, fewer microcracks were observed in the region of the crack tip. A region with a high density of fractured particles, similar to that observed on the surface of the specimen, was observed in this section. In addition, some unfractured ligaments between fractured areas were observed. These bridging ligaments

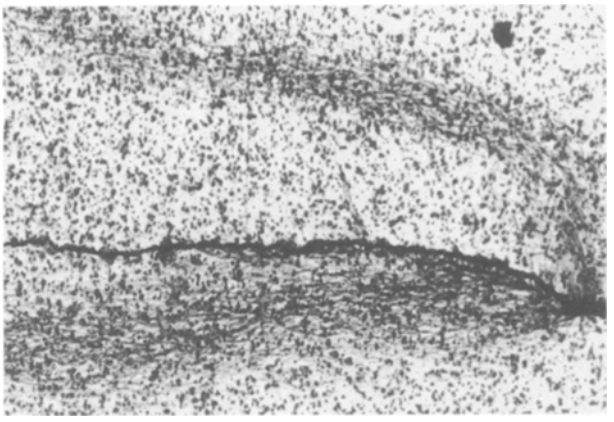

Figure 5 Optical micrograph illustrating the extensive microcracking associated with plane stress fracture. Note the presence of the shear bands originating from the crack tip, × 60.

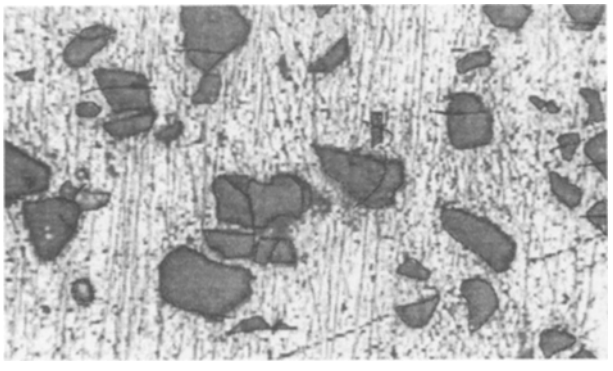

Figure 6 Ahead of the crack tip where microcracks cut through the particles, × 1000.

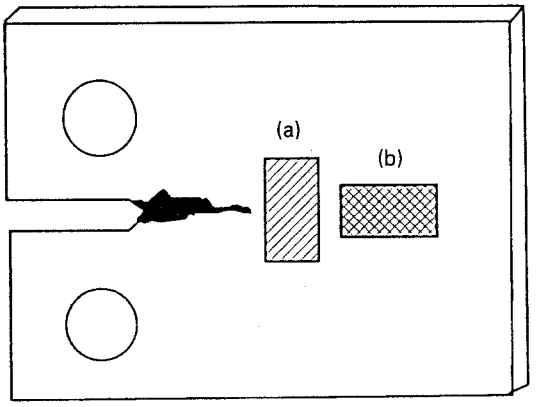

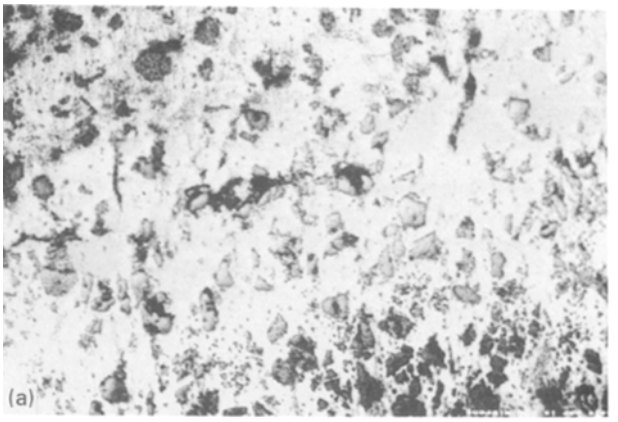

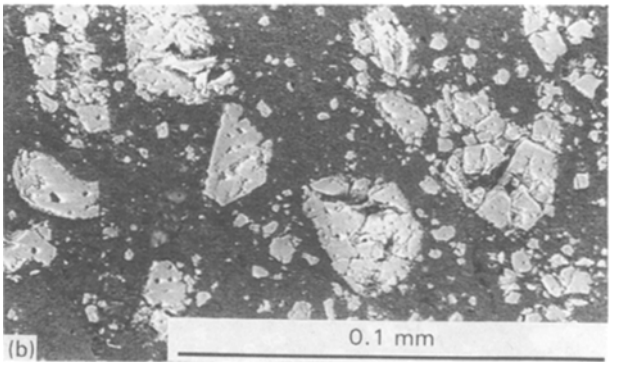

Figure 7 Region ahead of the crack tip containing a high density of fractured particles. (a) Laser confocal micrograph, × 300; (b) scanning electron micrograph.

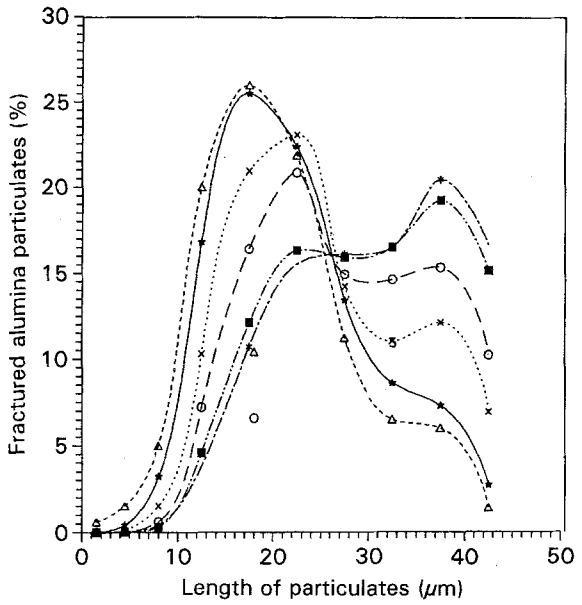

Figure 8 Size distribution of fractured particulates ahead of the crack tip on the CT specimen surface: (△) at crack tip, (★) 250 μm ahead of crack tip, (×) 500 μm ahead of crack tip, (○) 750 μm ahead of crack tip, (■) 1000 μm ahead of crack tip, (✳) 1250 μm ahead of crack tip.

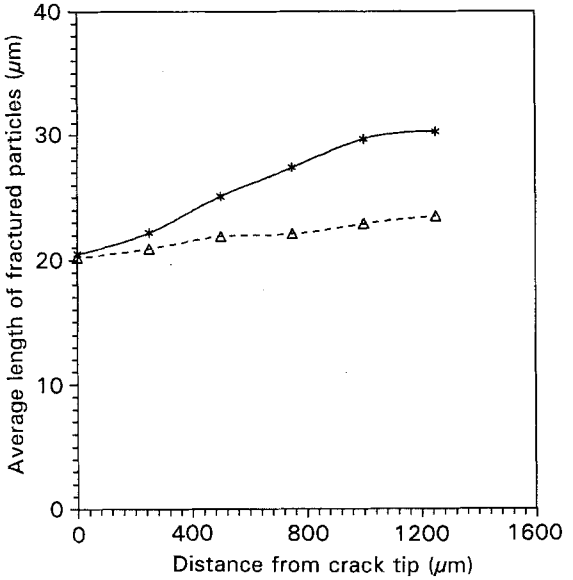

Figure 9 Average length distribution of fractured particulates as a function of distance ahead of the crack tip. (✳) surface, (△) mid-thickness.

TABLE II Comparison of the average geometric characteristic of the particulate phase in the as-received material with those of all fractured particles examined, both on the surface and mid-thickness regions

Condition	$\bar{L}_t$ (μm)	$\bar{A}_t$
As-received	18.7	1.8
Surface	23	2.8
Mid-thickness	22.2	2.7

are illustrated in Fig. 10a and b, which show, respectively, a large bridge near the crack tip and a bridge some distance from the crack tip, on the verge of failure. It was not possible to quantify the number of bridging elements or their size. Once broken, it was

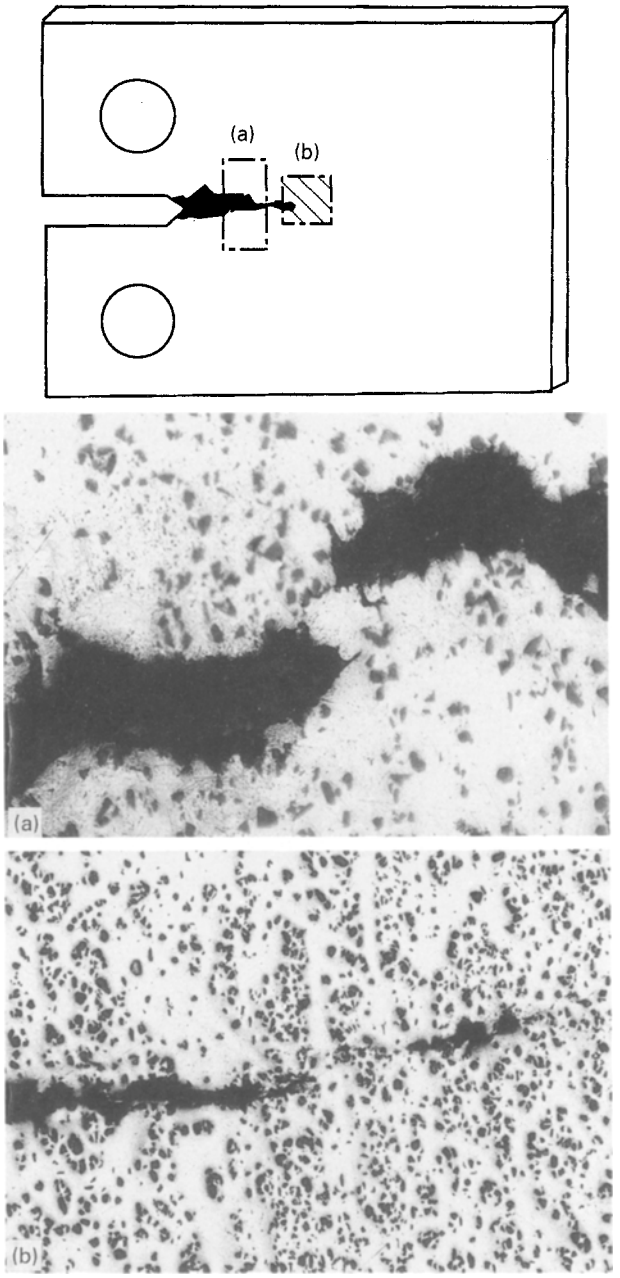

Figure 10 Bridging ligament associated with plane strain fracture (a) in the fractured area, ×250, (b) near the crack tip ×150.

unclear where the bridging elements had been located. A trend of increasing average fractured particle length with increasing distance from the crack tip was observed at both the surface and mid-thickness of the specimen; however, the average length in the mid-thickness was smaller (Fig. 9). In addition, the size distribution of fractured particles was different. While the most popular size range of fractured particles increased dramatically with increasing distance from the crack tip at the surface (Fig. 8), this change was much less marked in the mid-thickness region (Fig. 11). The percentage of small fractured particles under 5 μm in length in the mid-thickness region is about four times greater than on the surface of the specimen (Fig. 12b).

The results from Figs 8 and 11 indicate that particles with lengths smaller than 4 μm at the surface, and 3 μm in the mid-thickness of the specimen approximately 500 μm ahead of the crack tip, are rarely

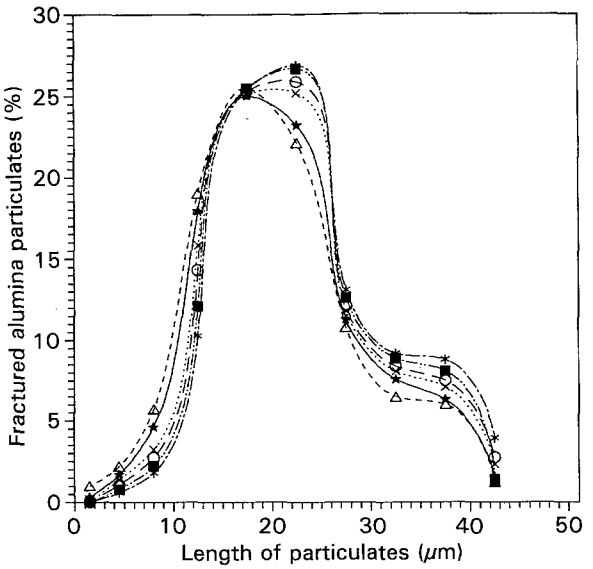

Figure 11 Size distribution of fractured particulates ahead of the crack tip in the CT specimen mid-thickness (symbols are the same as in Fig. 8).

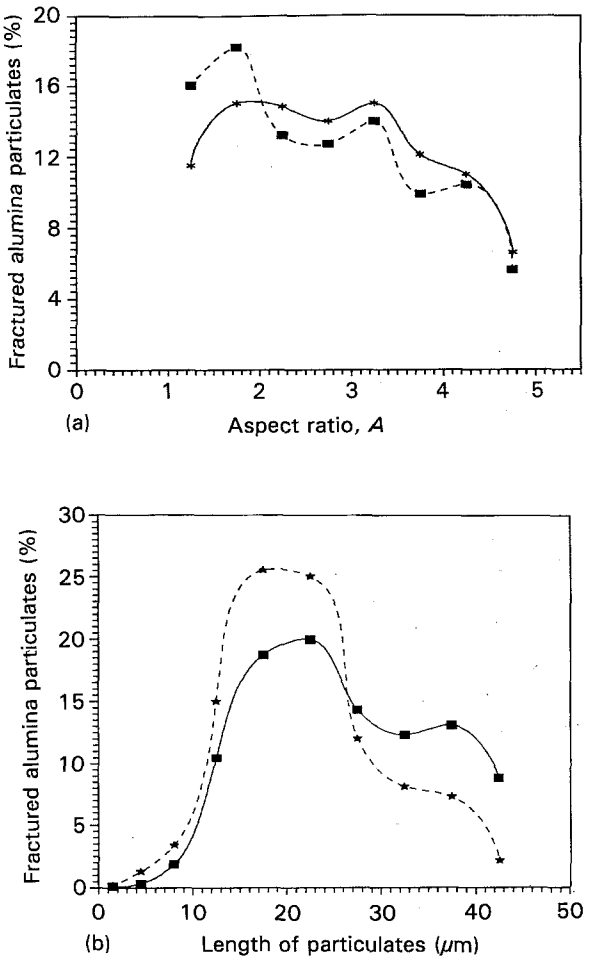

Figure 12 Average size distribution of fractured particulates on the surface and mid-thickness of CT specimen. (a) aspect ratio, (∗) surface, (■) mid-thickness; (b) length, (■) surface, (★) mid-thickness.

broken, and those in excess of 25 μm are almost all broken. Fig. 12a shows the aspect ratio distribution for the fractured particles. By comparing this figure with Fig. 3, it is clear that particles with higher aspect ratio, (elongated particles), are fractured preferentially.

3.3. Fractography

The fracture surface exhibited a ductile fracture morphology, consistent with void formation, growth and coalescence in the matrix phase. The primary dimples around broken alumina particles were deep and a few small secondary dimples were visible. Although some decohesion of particles from the matrix was evident, most of the particles were firmly embedded in the matrix (Fig. 13). Table III shows the results of image analysis on the fracture surfaces. The majority of the particulates on the fracture surface were fractured. The area of fractured particles was 11% which is considerably less than the reinforcement volume of 20%. The average size of the fractured particle was greater than the average particle diameter in the as-received condition, 21.6 μm compared to 18.7 μm.

4. Discussion

The fracture resistance of a material is proportional to the energy absorbed during the fracture process. There are several factors which contribute to energy absorption mechanisms in metal matrix composites and one of the most important is the plastic deformation within the plastic zone surrounding the crack tip. Most of the energy in this area is absorbed by the matrix. Hard and brittle alumina particles within the plastic zone of the growing crack reduce the amount of material that can plastically deform, leading to inhomogeneous deformation. Zener [10] suggested that extremely high local stresses could develop as the result of inhomogeneous deformation. High local stresses at the edge of alumina particles cause fracture and produce microcracks, thereby causing the area with a high density of fractured particles that was observed at a short distance from the main crack tip (Fig. 7). Cox and Low

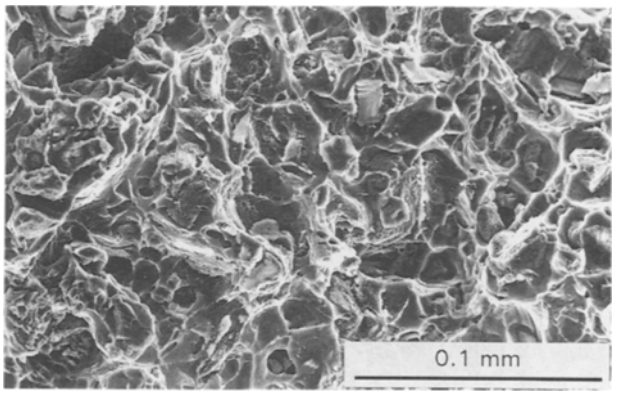

Figure 13 Scanning electron micrograph from fracture surface of CT specimen.

TABLE III Fractured surface particulate morphology, T6 condition

Material	Average fractured particles diameter (μm)	Area of fractured particles %	Inter particulate spacing (μm)	Fractured particles (%)
Duralcan 20%	21.6	11.2	11.1	74

[11] reported the same nucleation of microvoids at cleaved, hard particles in 18Ni maraging steel.

Although the fracture toughness results at crack initiation reported here satisfied all the size requirements of ASTM E399, it is clear that there are differences between the plane stress fracture at the surface and the plane strain fracture in the mid-thickness of the specimen at regions away from the crack tip. The technique of interrupting a fracture toughness test prior to complete fracture and examining the particulate response ahead of the crack tip is a very useful way of gaining insight into the fracture process and, in particular, the sequence of particle fracture which is not obtainable from examination of the fracture surfaces.

Extensive microcracking around the crack tip was observed on the specimen surface (Fig. 5). This distribution of microcracking would appear to be associated with the development of a shear tip. The microcracks in alumina particles some distance ahead of the crack tip propagate into the adjacent matrix with further straining, and generate a region with a large number of microcracks. The presence of a large number of microcracks near the main crack would effectively toughen the material [12]. The lower microcrack density in the plane strain condition compared to the plane stress region of the specimen is further evidence of this toughening effect.

Image analysis results show that the average size, $\bar{L}_t$, of the fractured particles is larger than the overall average particle size in the material (23 μm compared to 18.7 μm), on the specimen surface. Therefore, larger particles fracture more easily than small ones. The increasing average size of the broken particles with increasing distance from the crack tip shows that the large particles tend to fracture in the earlier stages of straining. Therefore, only larger particles appear to be effective sites for initial microcrack nucleation. The initiation of these microcracks must be assumed to be critical events in the fracture process. If one considers the particles that fracture in the earlier stages of straining as effective particles, the size range and volume fraction of these particles are critical values affecting the fracture mechanism. As the large and elongated particles tend to fail earlier during deformation, the probability of fracture increases rapidly with increasing size and aspect ratio of particles. Vanstone *et al.* [13] found the same phenomena and reported that void nucleation in 2xxx and 7xxx series aluminium alloys occurred first at the largest particles, and progressed to smaller and smaller particles as loading increases. It has been observed that the plastic strain necessary to fracture particles increases as particle size decreases, thus the smaller the particle size the better the damage tolerance at a given strength level [14]. The scarcity of fractured particles below 4 μm in the length (on both the surface and mid-thickness sections) is further evidence for the better tolerance of these particles. According to the results of this study, the particles with a length greater than 5 μm fracture earlier than other particles and may thus be considered as "effective" particles. On the other hand, particles smaller than 4 μm fracture at later stages of straining and they cannot be considered as effective particles (Fig. 8) and their effect on fracture toughness may be small. McClintock [15] proposed a model that predicts the fracture strain to be a function of the volume fraction of voids (initial void formers).

In contrast with surface observations, fewer microcracks were observed in the mid-thickness of the specimen. The difference in constraint would appear to influence the degree of microcracking. The presence of uncracked or bridging ligaments was only observed in the plane strain regions examined. It is not possible to determine the extent of these bridges through the specimen as only a two-dimensional observation has been made. It is, however, an energy absorption mechanism, which will therefore increase the crack resistance. This form of crack-interface bridging has also been reported in the brittle fracture of steel and alumina [16, 17] as well as in the fatigue of 7xxx series SiC particulate-reinforced composite [18].

The average length of fractured particles in the plane strain region was essentially the same as the plane stress region (at approximately 23 μm) but with more small particles (around 5 μm) fractured in the early stages of straining, (Fig. 12b). This indicates that the number of "effective" particles (those which produce voids earlier), in this section is markedly larger, and smaller particles can act as early void nucleation sites. Different states of stress between the surface and the centre of the specimen, together with different levels of residual stress due to quenching, result in the differences in the range of effective particles observed.

Further straining causes voiding in the fractured alumina particles and within the microcracks. The greater average length of these particles compared to the overall average length (21.6 μm compared to 18.7 μm) reinforces the fact that larger particles are more susceptible to fracture. Particles that initiated the microvoids are found at the bottom of dimples on the fracture surface (Fig. 13). Voids that form during fracture are found as dimples on the fracture surface. The growth and coalescence of these microvoids is another important energy-absorption mechanism. Fig. 14 shows the sequence of failure in Duralcan-20% MMC. This sequence has largely been determined from observations made ahead of the crack tip in the interrupted fracture test. Initial straining causes some previously unbroken particles (a) to fracture (b); further straining causes more particle fracture and multiple fracture of individual particles (c) with the onset of voiding and cracking in the matrix (d). These cracks and voids start to coalesce (e) before linking up with the main crack (f) resulting in fracture and catastrophic failure.

5. Conclusions

1. In the reinforcement phase of a MMC, only those particles which nucleate voids early in the fracture process ahead of the crack tip may be considered to be effective particles. The size and volume fraction of these particles are critical in defining the fracture toughness.

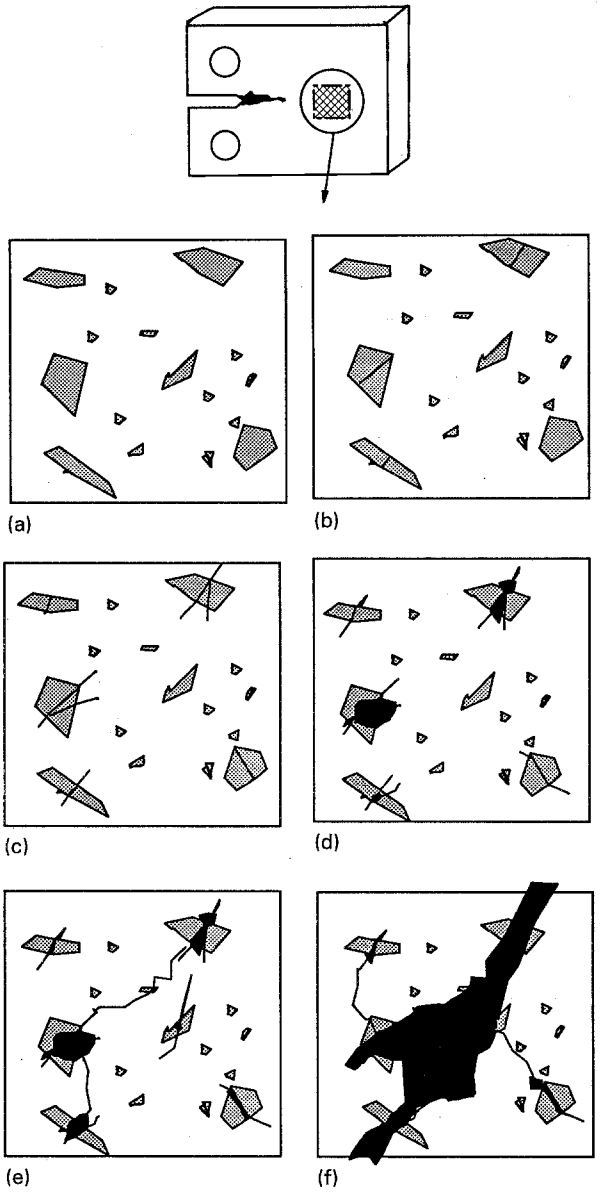

Figure 14 Sequence of fracture in Duralcan-20%.

2. The dominant fracture mechanism in Duralcan-20% is particle fracture. Fractured particles act as void-initiation sites and fracture occurs after growth and linkage of the voids.

3. The response of particles on the surface and in the mid-thickness (plane strain as opposed to plane stress) is different.

4. Larger and more elongated particles are more susceptible to fracture than smaller particles. These particles nucleate microcracks earlier than small particles, thus reducing the fracture resistance of the composite. Therefore, decreasing the range and average size of the reinforcement phase would result in increased toughness.

5. Microcrack formation and crack bridging are mechanisms which would increase the fracture resistance of Duralcan-20% MMC material; the former acting in the plane stress condition and the latter in the plane strain condition.

Acknowledgements

The authors thank the Australian Research Council (ARC) for the continuing support of this project. M. J. Hadianfard is supported by a junior Research Fellowship funded by the ARC.

References

1. A. P. DIVECHAN, S. G. FISHMAN and S. D. KARMARKAR, *J. Metals* **33** (1981) 12.
2. R. J. ARSENAULT, *Mater. Sci. Eng.* **64** (1984) 171.
3. D. L. McDANELS, *Metall. Trans.* **16 A** (1985) 1105.
4. D. L. DAVIDSON, *ibid.* **18** (1987) 2115.
5. Y. FLOM and R. J. ARSENAULT, *Acta Metall.* **37** (1989) 2413.
6. T. G. NIEH, J. WADSWORTH and D. J. CHELLMANN, *Scripta Metall.* **19** (1985) 181.
7. S. R. NUTT and A. NEEDLEMAN, *Scripta Metall.* **21** (1987) 705.
8. J. P. LUCAS, P. K. LIAW and J. J. STEPHENS, in "Morris E. Fine Symposium", Detroit, Michigan, October, 1990. (The Minerals, Metals and Materials Society, 1991) p. 171.
9. M. MANOHARAN and J. J. LEWANDOWSKI, *Scripta Metall.* **23** (1988) 1801.
10. C. ZENER, "Fracturing of Metals" (ASM, Cleveland, OH, 1948) p. 3.
11. T. B. COX and J. R. LOW, *Metall. Trans.* **5** (1974) 1457.
12. D. L. DAVIDSON, in "Metal Matrix Composites Mechanisms and Properties", edited by R. K. Everett and R. J. Arsenault, (Academic Press, Boston, 1991) p. 217.
13. R. H. VANSTONE, R. H. MERCHANT and J. R. LOW, ASTM STP 556 (American Society for Testing and Materials, Philadelphia, PA, 1974) p. 93.
14. D. BROEK, *Eng. Fract. Mech.* **5** (1973) 55.
15. F. M. McCLINTOK, *Int. J. Fract. Mech.* **2** (1966) 614.
16. A. R. ROSENFIELD and B. S. MAJUMDAR, *Metall. Trans.* **18 A** (1987) 1053.
17. Y. W. MAI and B. R. LAWN, *J. Am. Ceram. Soc.* **70** (1987) 289.
18. J. K. SHANG and R. O. RITCHIE, *Metall. Trans.* **20 A** (1989) 897.
19. T. LYMAN, "Metal Handbook", Vol. 1, 8th Edn. (American Society for Metals, Metal Park, OH, 1961) p. 964.

Received 25 May
and accepted 1 November 1993